Microchemical Journal 222 (2026) 117277

Contents lists available at ScienceDirect

Microchemical Journal

journal homepage: www.elsevier.com/locate/microc

Integrated pharmacokinetic and tissue-distribution profiling of rhein in mice, and its modulation of endogenous metabolism in liver and kidney revealed by LC-MS/MS and DESI-MSI

Qin Shen [a,b,c,1], Longhui Zhang [b,1], Chuting Xu [b], Guosheng Fu [b], Qinying Feng [b], Yongli Wang [c], Chaoqun Zhao [b], Wenna Ma [d], Hong Xu [c,*], Wei Liu [a,b,c,*], Jing Hu [a,*]

[a] Department of Nephropathy, The Seventh People's Hospital affiliated to Shanghai University of Traditional Chinese Medicine, Shanghai 200137, China
[b] Department of pharmacy, The NATCM Third Grade Laboratory of Traditional Chinese Medicine Preparations, Shuguang Hospital Affiliated to Shanghai University of Traditional Chinese Medicine, Shanghai 201203, China
[c] Institute of Chinese Materia Medica, Shanghai University of Traditional Chinese Medicine, The MOE Key Laboratory for Standardization of Chinese Medicines, Shanghai 201203, China
[d] Hebei Chemical & Pharmaceutical College, Hebei 050026, China

ARTICLE INFO

Keywords:
Rhein
LC-MS
DESI-MSI
Pharmacokinetics
Tissue distribution
Metabolites

ABSTRACT

Rhein, an anthraquinone derivative, has been confirmed by contemporary research to possess substantial bioactivity and clinical potential in. However, its spatiotemporal distribution patterns within the body remains poorly understood. This study employed an integrated approach combining liquid chromatography-tandem mass spectrometry (LC-MS/MS) with desorption electrospray ionization mass spectrometry imaging (DESI-MSI) spatial metabolomics to evaluate the spatiotemporal heterogeneous distribution characteristic and metabolic remodeling effects of rhein in liver and kidney tissues. Through the establishment of a validated LC-MS/MS quantification system, we analysized the distribution profiles of rhein in plasma, liver, and kidney samples. Pharmacokinetic analysis revealed that rhein rapidly reached its peak concentration within 0.17 h, was subsequently metabolized in the liver and ultimately excreted *via* the kidneys. Further analysis using DESI-MSI to map the spatial distribution of rhein and its endogenous metabolites demonstrated that rhein was initially concentrated primarily in the renal cortex and gradually accumulated in both the cortex and medulla regions over time. Subsequently, relative metabolic pathways indicated that rhein affected amino acid, carbohydrate metabolic pathways and phospholipid metabolism in liver and kidney tissues. Furthermore, the representative mRNA associated with the lipid metabolism showed that oral administration of rhein may affect lipid metabolism. This present work offers a novel framework for elucidating the tissue distribution characteristics and underlying mechanisms of action of natural products.

1. Introduction

Natural products (NPs) represent a vast treasure trove and critical source for drug discovery worldwide [1]. Traditional Chinese medicine (TCM) theory posits that naturally derived chemicals, by virtue of their molecular structure, can exert potent therapeutic effect [2]. Indeed, more than half of all small-molecule in current clinical use are directly or indirectly inspired by NPs [3]. Among these, rhein, an anthraquinone compound, demonstrates pronounced bioactivity and broad clinical utility. Diacerein, a front-line IL-1 inhibitor for osteoarthritis, was developed from rhein [4]. Moreover, rhein has been widely applied to pneumonia [5], arthritis [6] and in the barrier dysfunction [7]. Recent pharmacological studies further revealed that rhein protects the liver and kidneys through anti-fibrotic, lipid-lowering, and anti-

* Corresponding authors at: Department of pharmacy, Department of Nephropathy, The Seventh People's Hospital affiliated to Shanghai University of Traditional Chinese Medicine, Shanghai 200137, China (J. Hu). The NATCM Third Grade Laboratory of Traditional Chinese Medicine Preparations, Shuguang Hospital Affiliated to Shanghai University of Traditional Chinese Medicine, Shanghai 201203, China(W. Liu). Institute of Chinese Materia Medica, Shanghai University of Traditional Chinese Medicine, The MOE Key Laboratory for Standardization of Chinese Medicines, Shanghai 201203, China (H. Xu).
E-mail addresses: xuhongtcm@shutcm.edu.cn (H. Xu), lwhzayl@163.com (W. Liu), 6264570@qq.com (J. Hu).
[1] Qin Shen and [1] Longhui Zhang were contributed equally to this work

https://doi.org/10.1016/j.microc.2026.117277
Received 8 October 2025; Received in revised form 1 February 2026; Accepted 3 February 2026
Available online 5 February 2026

inflammatory properties [8]. In a murine model, Xia Yu Decoction—of which rhein is a key component—significantly attenuated carbon-tetrachloride-induced liver fibrosis [9]. Rhein has also been found to alleviate CCl_4-induced liver fibrosis, methotrexate-driven chronic liver injury [10], and effectively reverse nonalcoholic fatty liver disease by lowering hepatic lipids and inflammation [11]. Similarly, Xiexin Decoction'active fractions-rich in rhein-attenuates renal fibrosis in db/db diabetic mice [12]. Although, the protective effects of rhein on the liver and kidneys are well documented, its precise molecular mechanism remains elusive, elucidating its *in vivo* pharmacokinetics and tissue distribution is therefore essential. Pharmacometabonomics, which captures endogenous metabolites and other exposure markers [13], has matured into a key technology for modern drug discovery and for dissecting the polypharmacology of traditional Chinese medicines [14]. To understand how rhein exerts its action, its *in vivo* pharmacokinetics profile and spatial distribution characteristics within tissues must be resolved. Although plasma pharmacokinetics and distribution of rhein in liver and kidney have been described [15], conventional assays lack the spatial resolution for metabolic visualization and cannot reveal the characteristics of tissue microdistribution and spatial and temporal dynamics of metabolism [16].

Mass spectrometry imaging (MSI) is rapidly advancing metabolomics, lipidomics, and proteomics by furnishing label-free, high-resolution molecular maps without laborious extraction or separation- an asset particularly valued for complex TCM [17]. In combination with chemometric methods, MSI can identify potential pharmacodynamics and toxicodynamic biomarkers directly within tissue and explore the therapeutic and toxicity mechanisms of TCM [18]. When integrated into global metabolomics workflows, these spatial data accelerate drug discovery, repurposing and interaction studies [19]. Currently, the integration of multi-omics with spatial MSI technology has emerged as a research trend that facilitates the exploration of drug treatment mechanisms for certain diseases. Chen et al. (2024) employed MSI-based spatial metabolomics with liver-specific transcriptomics to analyze how *Eclipta eclipta* bioactives reprogram lipid metabolism and protect against nonalcoholic fatty liver disease (NAFLD) [20]. Similarly, Han et al., (2025) coupled high-throughput UPLC-MS/MS with MSI driven metabolomics technology to achieve precise localization of the spatial distribution of core biomarkers and drug active ingredients in kidney tissue of Huangkui capsule [21]. MSI combined with multi-omics analysis facilitates the identification of potential drug targets and offers novel insights into molecular mechanisms.

The pre-treatment process of traditional mass spectrometry will destroy the original structure of the sample and lose spatial information. The LC-MS/MS can perform high-precision absolute quantification of analytes in tissues, but it cannot resolve spatial distribution information. In contrast, DESI-MSI can perform *in situ* spatial localization. MSI only requires attaching tissue sections to a glass slide and conducting *in situ* detection directly. DESI-MSI also has certain limitations. DESI-MSI is more suitable for the analysis of small molecules with moderate polarity, as these substances can be effectively ionized under the DESI conditions. However, for highly polar or large-molecule analytes (such as peptides and proteins), the signal sensitivity of DESI will decrease, thereby limiting the application of this method. Currently, there are relevant reports on the study of the exposure of rhein, but there is still a lack of *in situ* visualization. So the strategic innovation of this study lies in the unprecedented integration of DESI-MSI spatial metabolomics with LC-MS quantitative pharmacokinetics, systematically revealing the spatial and temporal heterogeneity of rhein distribution in the liver and kidney, as well as its metabolic remodeling effects. The LC-MS/MS quantitative verification system was further established to analyze rhein concentrations in the plasma, liver, and kidney tissue of mice following oral administration of rhein. The spatial dynamics of rhein metabolites within the kidney cortex/medulla and liver lobular were analyzed by DESI-MSI technology. Using open-source software, combining endogenous metabolites can help explore potential mechanisms and metabolic pathways. This study strategy is showed in Fig. 1A, providing a novel paradigm for investigating the tissue distribution and potential mechanism of action of NPs.

2. Materials and methods

2.1. Chemicals and reagents

Rhein was purchased from Dalian Meilun Biotechnology Co., Ltd. (Dalian, China). High-performance liquid chromatography (HPLC)-grade methanol, acetonitrile, and formic acid were obtained from Fisher Scientific (Santa Clara, USA). Ultrapure water was supplied by Hangzhou Wahaha Group Co., Ltd. (Hangzhou, China). Leucine enkephalin was acquired from Waters Corporation (Milford, US). Sodium formate and 903™ Protein Saver Cards were purchased from Merck (NJ, USA).

2.2. Animal experiments

A total of 35 male C57 BL/6 J mice (18–22 g) were provided by the Shanghai SlAC Laboratory Animal Co. Ltd. and housed in the Experimental Animal Center of Shanghai University of Traditional Chinese Medicine (Permit Number: SCXK (Hu) 2022–0004). The experimental protocol was approved by the Animal Ethics Committee at Shanghai University of Traditional Chinese Medicine (Approval Number: PZSHUTCM2505090005). The animals were raised under controlled conditions (22 °C ± 2 °C, 40% relative humidity, 12 h light/dark cycle) with free access to food and water.

2.3. Quantitative analysis of rhein in biological samples by LC-MS/MS

2.3.1. LC-MS analysis conditions

The analyte rhein was quantified by LC-MS on an ACQUITY UPLC™ BEH C_{18} column (50 mm × 2.1 mm, 1.7 μm) maintained at 40 °C. The flow rate was 0.4 mL/min and the injection volume was 3 μL. Mobile phase A was 0.1% formic acid aqueous solution, and mobile phase B was acetonitrile. The gradient elution was performed as follows: 0–0.5 min, 95% A; 0.5–2.5 min, 95%–55% A; 2.5–3.5 min, 55%–5% A; 3.5–5.0 min, 5% A; 5.0–5.1 min, 95% A; and 5.1–6.0 min, 95% A. Mass spectrometric detection was performed in negative electrospray mode. The ion spray voltage was −4500 V, the turbo spray temperature was 500 °C, the deisolation potential (DP) was −20 V, and the collision energy (CE) was −40 eV. Nitrogen served as nebulizer and auxiliary gas. The gas pressures for the nebulizer (gas 1), heater (gas 2), and curtain gas were 40, 50, and 35 pounds per square inch, respectively. The full scan spectra were acquired from *m/z* 100 to m/z 1000 with an cumulative duration of 200 ms. The study employed the key parameter collision energy distribution (CES) to maximize sensitivity and minimize the information loss. Data were processed with MultiQuant MD 3.0.3.

2.3.2. Tissue distribution after oral administration of rhein

Mice were randomly divided into seven groups ($n = 5$) according to different time points at 0, 0.17, 0.5, 1, 2, 4, and 8 h after oral administration. Before the experiment, all animals were fasted without water. The mice were administered rhein (100 mg/kg) in 0.4% (*w/v*) sodium carboxymethyl cellulose for the single-dose study. At each time point, animals were anesthetized with 3% pentobarbital sodium prior to sacrifice. Plasma was collected into heparinized tubes, and 20 μL of plasma were immediately spotted onto 903™ Protein Saver Cards. Kidney and liver were excised, snap-frozen in dry ice, and stored at −80 °C for subsequent analysis. At the same time, as commercial authentic standards of M-R-O-G were unavailable, we used the rhein semi-quantitative method for the detection.

2.3.3. Sample preparation

To prepare calibration standards (CS) and quality-control (QC) samples, 100 μL of blank plasma was mixed with 100 μL working

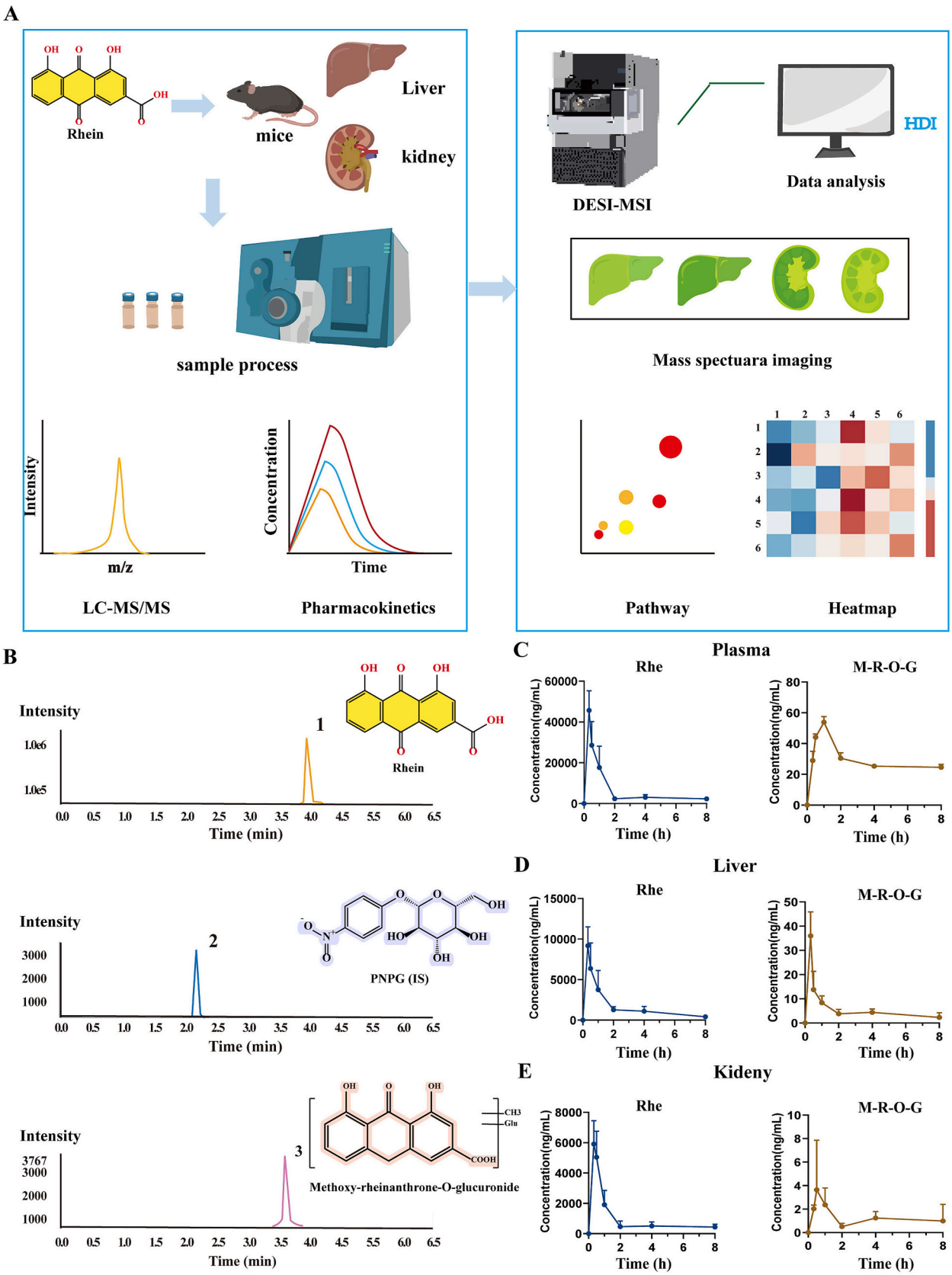

Fig. 1. The work flow of this study and LC-MS/MS analysis. (A) Research strategy for spatially-resolved metabolomics in rhein. (B) LC-MS/MS of rhein, IS and methoxy-rheinanthrone-O- glucuronide. (C-E) Peak area-time curve of rhein and its metabolites in plasma (C), liver (D), and kidney (E) analyzed by LC-MS/MS.

solution (CS or QC), 10 μL ascorbic acid and 100 μL ultrapure water. 100 μL of acetonitrile containing the 100 ng/mL of internal standard (IS) was then added. The plasma sample to be tested was processed as described above. After vortex-mixing for 60 s, the mixture was centrifuged at 12,000 ×*g* for 15 min. A 150 μL of the supernatant was transferred to an liquid vial, and 3 μL was injected for LC-MS analysis.

2.4. Methodological analysis of LC-MS/MS

The quantitative method was validated for linearity, accuracy, precision, stability, and matrix effect in accordance with the US Food and Drug Administration (FDA) Bioanalytical Method Validation Guidance (Food and Drug Administration, 2022).

2.4.1. Linearity and lower limit of quantification (LLOQ)

A series of mixed references and IS solutions was added to the blank rat plasma and tissue homogenates for subsequent analysis. The calibration curves were established by plotting the concentration of each reference substance (X) against the peak area ratio of the analytes to the IS (Y). LLOQ was defined as the lowest concentration yielding a signal-to-noise ratio of 10, with the acceptable accuracy within 80%–120%.

2.4.2. Precision and accuracy

Accuracy and precision were assessed through both intra-day and inter-day analyses. QC samples at low, medium, and high concentrations were analyzed in six replicates within a single day to evaluate intra-day accuracy and precision. The same QC levels were analyzed daily over three consecutive days to evaluate intra-day accuracy and precision.

2.4.3. Stability

To assess the stability of analytes, QC samples were subjected to three distinct storage conditions: 4 °C for 24 h, repeated freeze-thaw cycles, and long-term storage at −80 °C. For 24-h stability, low-, medium-, and high - concentration QC samples were held at 4 °C for 24 h. Freeze-thaw stability, was assessed by subjecting samples to three complete freeze-thaw cycles at (−20 °C to room temperature) over consecutive days, followed by analysis to detect any analyte changes. For long-term stability, QC samples were kept at −20 °C for 15 days and analyzed after thawing to evaluate analyte integrity.

2.4.4. Extraction recovery and matrix effect

Recovery and matrix effect were assessed using six replicate QC samples at low, medium, and high concentrations. An aqueous solution was replaced plasma for the recovery assessment. The QC samples were processed and analyzed in accordance with the sample treatment methodology. The ratio of the analyte peak area ratio to the IS was designated as A. Blank plasma was processed identically after with reference solutions for analysis. The peak area ratio of the compound to IS was recorded as B, and recovery was the percentage of peak area ratio of A to B. Subsequently, 80% methanol-acetonitrile solution was selected as the blank tissue extract, and the peak area ratio of each compound to the IS was recorded as C. The matrix effect was expressed as the percentage of the peak area ratio between A and C, required to fall within 85–115%.

2.5. Spatial metabolomics analysis by DESI-MSI

Frozen kidney and liver tissues were cut into 10 μm sections using a Leica CM CM3050S freezing microtome at −20 °C. Thawed sections were mounted on positively charged slides, sealed and stored at −80 °C. Prior to analysis, slices were dried for 30 min at −20 °C in a vacuum dryer. DESI-MSI was performed in negative resolution mode (20,000 FWHM at *m/z* 100–1000) and equipped with a 2D DESI XS source. The solvent for the spray application was an methanol/water (95:5) at 5 μL/min. The spray voltage was 3 kV, the N_2 gas pressure was 0.4 MPa, and the pixel size for DESI-MSI scanning was set at 100 μm × 100 μm.

Data were obtained using MassLynx™ software version 4.2 (Waters Corporation, Milford, MA, USA). The acquisition and processing of imaging data were conducted using high-definition imaging (HDI) software V1.6 (Waters Corporation, Milford, MA, USA).

2.6. Methodological analysis of DESI-MSI

The key parameters of the DESI-MSI platform include tests such as flow rate, stability, linearity, detection limit, quantification limit, and intra-day precision. By using adjacent slices of collected blank kidney and liver tissues to enhance the *in situ* detection of rhein and its endogenous metabolites in kidney and liver tissues. Comparisons were made between spray flow rates of 3 μL/min and 5 μL/min, as well as spray solvents of methanol/water (95:5) and acetonitrile/water (80:20). At the same time, we evaluated the stability of the DESI-MSI system by analyzing adjacent kidney and liver slices over three consecutive days. We evaluated the inter-day precision of low concentration quality control (QCL), medium concentration quality control (QCM) and high concentration quality control (QCH). For each concentration, we scanned 6 times on consecutive blank liver and kidney slices within a day. And Additionally, we spotted 0.2 μL of standard solutions of rhein at different ratios on blank kidney and liver adjacent slices, with concentrations of 0.31, 0.625, 1.25, 2.5, 5, and 10 μg/mL (each drop dried area was approximately 2.21 square millimeters), to further investigate the quantitative capability of the proposed method. The lowest detection limit (LOD) needs to satisfy a signal-to-noise ratio (S/N) of ≥3, and the lowest quantification limit (LOQ) needs to satisfy a S/N of ≥10.

2.7. Sample prepartion of DESI-MSI

The collected plasma was dropped onto a 903TM protein preservation card in 20 μL. The kidneys and liver were quickly placed in dry ice for frozen, and then stored at −80 °C until analysis. The Leica CM 3050S cryostat (Leica Microsystem Ltd., Germany) was used to cut the tissues into 10 μm sections at −80 °C. After the sections were thawed, they were placed on a positively charged desorption plate (Thermo Scientific, California, USA) and stored in a sealed container at −80 °C until further analysis. The plates were transferred to −20 °C for overnight storage before analysis. Then, plates were taken out from −20 °C and subjected to vacuum drying for half an hour for DESI-MSI analysis.

2.8. Data analysis in LC-MS/MS and DESI-MSI

LC-MS/MS data were processed with Multiquant 3.0 to analyze the plasma drug concentration. Pharmacokinetic parameters were obtained by fitting and computation using the Lixoft monolix Suite 2024R. Data acquisition and spectral analysis were conducted using MassLynx™. DESI ion images were generated in HDI V1.6. The dataset was obtained using total ion counts, with lipid identification based on accurate mass facilitated by LIPID MAPS databases (https://www.lipidmaps.org) and the Human Metabolome Database (HMDB) (http://hmdb.ca/). We placed the imaging data of the standard lipid metabolite samples (PE (18:0/18:2(9Z,12Z) and TG(36:0)) that we can purchase in the Fig. S1A-S1B. Regions of interest (ROIs) were created ($n = 3$), and HDI™ software was used to analyze the spatial lipid distribution in the liver. For each of the seven chromatograms, the sum of the total ion intensities was calculated, and the obtained data matrix was imported into SIMCA 14.1, and principal component analysis (PCA) and orthogonal partial least squares discriminant analysis (OPLS-DA) were performed. Path analysis focused on lipids showing significant differences across the three study areas. Additionally, metabolic pathway data was obtained from MetaboAnalyst 6.0 (https://www. Metaboanal yst .ca/). Statistical analysis was performed using GraphPad Prism software. Data were presented as mean ± standard deviation (SD). One-way analysis of variance (ANOVA) was followed by Tukey tests to determine the statistical significance between groups. $P < 0.05$ is considered to be

statistically significant.

2.9. Real-time quantitative PCR

The liver and kidney tissues (30 mg) were used Trizol standard procedures to extract total RNA ($n = 4$). Subsequently, cDNA synthesis was carried out according to the operation of Takara PrimeScript RT kit. GAPDH was used as the standard control gene, and the relative mRNA expression levels of all genes were analyzed by comparing the CT values. The primer sequences were detailed in the Supplementary material Table S1.

3. Results and discussion

3.1. LC-MS/MS analysis of the pharmacokinetics and tissue distribution of rhein in the liver and kidney

3.1.1. Optimization of LC-MS/MS conditions

Biological samples were processed by protein precipitation, and plasma samples were treated with methanol. Chromatographic conditions were optimized to a 6 min gradient using 0.1% formic acid aqueous solution and acetonitrile (B) as the mobile phase. MS parameters, such as CE and cone hole voltage (CV), were optimized to achieve the maximum response (Table S2).

3.1.2. Method validation

Fig. 1B presents the representative MRM chromatogram of plasma collected after oral administration of rhein, which contained isothiocyanates with IS of 25.00 ng/mL. The calibration curve of rhein showed a linear relationship within the concentration range of 1.31–800 ng/mL (Rhein: $Y = 0.2341\times + 0.1447$, $R^2 = 0.9960$). The LOD of rhein was 0.63 ng/mL, and the LLOQ of rhein was 1.31 ng/mL. Accuracy, precision, matrix effect, and stability data are summarized in Tables S3-S5: intra- and inter-day RSD $\leq$ 15%, accuracy 89.10–109.78%, with acceptable matrix effect and stability.

3.1.3. Plasma pharmacokinetics and liver/kidney tissue distribution characteristics of rhein and its metabolites by LC-MS/MS

The validated LC-MS/MS method was used to quantify rhein and its metabolites in plasma, liver, and kidney of mice. Figs. 1C-1E present the plasma concentration - time curves of rhein and its main metabolite, methoxy-rheinanthrone-O-glucuronide (M-R-O-G)) [22], following a single oral administration of 100 mg/kg rhein. The concentrations of rhein in plasma, liver, and kidney are listed in Tables S6 and S7. Pharmacokinetic parameters are summarized in Table 1. The plasma concentration of rhein showed a gradual decline trend with $T_{1/2}$ of 3.28 ± 1.88 h. C_{max} and $AUC_{(0\text{-}t)}$ of rhein in the plasma were 49,936.62 ± 10,216.21 ng/mL and 54,459.59 ± 15,740.11 ng·h/mL, respectively.

Table 1
Pharmacokinetic parameters of rhein in plasma, liver, and kidney (mean ± SD, $n = 5$).

Pharmacokinetics parameters	Plasma	Liver	Kidney
ke (/h)	0.25 ± 0.11	0.24 ± 0.14	0.19 ± 0.06
$T_{1/2ke}$ (h)	3.28 ± 1.88	3.70 ± 1.56	4.08 ± 1.32
C_{max} (ng/mL)	49,936.62 ± 10,216.21	9546.86 ± 2814.51	6295.19 ± 1619.78
$AUC_{(0\text{-}t)}$ (ng·h/mL)	54,459.59 ± 15,740.11	13,862.06 ± 4597.57	8168.54 ± 872.78
$AUC_{(0\text{-}\infty)}$ (ng·h/mL)	68,979.80 ± 14,842.59	16,454.28 ± 4361.56	1110.47 ± 1651.91
MRT (h)	2.80 ± 0.40	2.08 ± 0.23	2.27 ± 0.37
V_d (mL/kg)	6836.92 ± 3368.37	33,429.16 ± 13,616.56	51,778.09 ± 9647.29
CL (mL/h/kg)	1501.41 ± 361.33	6385.17 ± 1960.54	9106.33 ± 1394.21

Rhein reached peak concentrations of 9546.86 ± 2814.51 ng/mL and 6295.19 ± 1619.78 ng/mL in the liver and kidney, respectively. C_{max} and $AUC_{(0\text{-}t)}$ of rhein in the liver and kidney were higher than those in the plasma. Thus, rhein was absorbed mainly in the plasma. The plasma concentration of rhein showed a rapid decline, with $T_{1/2}$ of 3.28 ± 1.88 h and $T_{1/2}$ of 3.70 ± 1.56 h in the liver. However, $T_{1/2}$ and MRT of rhein in the kidney were 4.08 ± 1.32 h and 2.27 ± 0.37 h, respectively, which were lower than those of rhein in the plasma. This result suggested that rhein was eliminated more slowly in the plasma than in the liver and kidney. *CL* of rhein in the kidney was 9106.33 ± 1394.21 mL/h/kg higher than in the plasma and liver. Thus, rhein was metabolized in the liver and excreted in the kidney. The pharmacokinetic parameters of M-R-O-G as the metabolite were investigated (Table S8). C_{max} and $AUC_{(0\text{-}t)}$ of M-R-O-G in the plasma were 55.04 ± 2.91 ng/mL and 237.41 ± 8.95 ng·h/mL, respectively, which were higher than those of rhein in the liver and kidney. Thus, the concentration of M-R-O-G was lower than that of rhein, reaching the peak concentration in the plasma at 1 h.

3.2 Analysis of the pharmacokinetics and distribution of rhein in the liver and kidney by DESI-MSI.

3.1.4. Optimization of conditions for DESI-MSI analysis

Flow rates were optimized to enhance *in-situ* detection of rhein and its endogenous metabolites. The flow rate was compared using the spray solvent at 3 and 5 μL/min. The results revealed that 5 μL/min (spray solvent: 95:5, *v/v* MET/H_2O) yielded higher signal intensity than 3 μL/min (Figs. S2A-S2D) and was therefore selected for DESI-MSI. About 0.2 μL of the standard rhein was applied at concentrations of 0.31, 0.625, 1.25, 2.5, 5, and 10 μg/mL onto blank liver and kidney sections (the area of each point after droplets dried was approximately 2.21 mm^2). The resulting densities of the standard rhein at corresponding spots were 0.14, 0.28, 0.57, 1.13, 2.26, and 4.52 ng/mm^2. The standard curve of rhein was established by plotting the average ion intensities of ROIs. All concentrations were successfully detected in $[M]^-$ ion at *m/z* 283.01 (Figs. S2E-S2F). The calibration curve demonstrated good linearity with a correlation coefficient (R^2) of 0.9940 and 0.9975 (Figs. S2G-S2H), confirming that the method meets analytical requirements. Subsequently, the stability was analyzed over three consecutive days. RSD was 8.29% and 12.90% which showed in Figs. S1I-S1L. The LOD of rhein was 0.1 μg/mL, and the LOQ of rhein was 0.31 μg/mL (Figs. S3A-S3B). Finally, the intra-day precision was showed in Figs. S3C-S3D with RSD $\leq$ 15% in QCL (0.625 μg/mL), QCM (1.25 μg/mL), QCH (10 μg/mL).

3.1.5. Spatial distribution characteristics of rhein and its metabolites in tissues

The spatiotemporal distribution of rhein after oral administration were mapped by the optimized DESI-MSI method. The response of rhein in plasma was higher than that in liver, and kidney (Fig. 2). After oral administration, rhein was detected at 0.17 h in plasma, liver, and kidney, indicating its rapid systemic distribution. No obvious tissue specificity was observed in plasma or liver. The kidney was subdivided into renal cortex, renal medulla, and renal pelvis. Figs. 2A-2B showed that rhein initially spread rapidly through cortical region, then gradually accumulated in both the cortex and medulla, falling below the limit of detection 8 h after administration. The content of rhein in the liver and kidney was relatively low, indicating that rhein was metabolized by the liver, reabsorbed by the kidney, and excreted from the body *via* urine. The metabolite M-R-O-G was not detectable in plasma at any point, and rhein was present at higher levels than M-R-O-G in both liver and kidney (Figs. 2C-2D). M-R-O-G was rapidly distributed throughout the body, but its concentrations in the kidney and liver remained low. Both rhein and M-R-O-G reached peak concentration at 0.17 h after administration, thereafter M-R-O-G declined and became undetectable after 2 h.

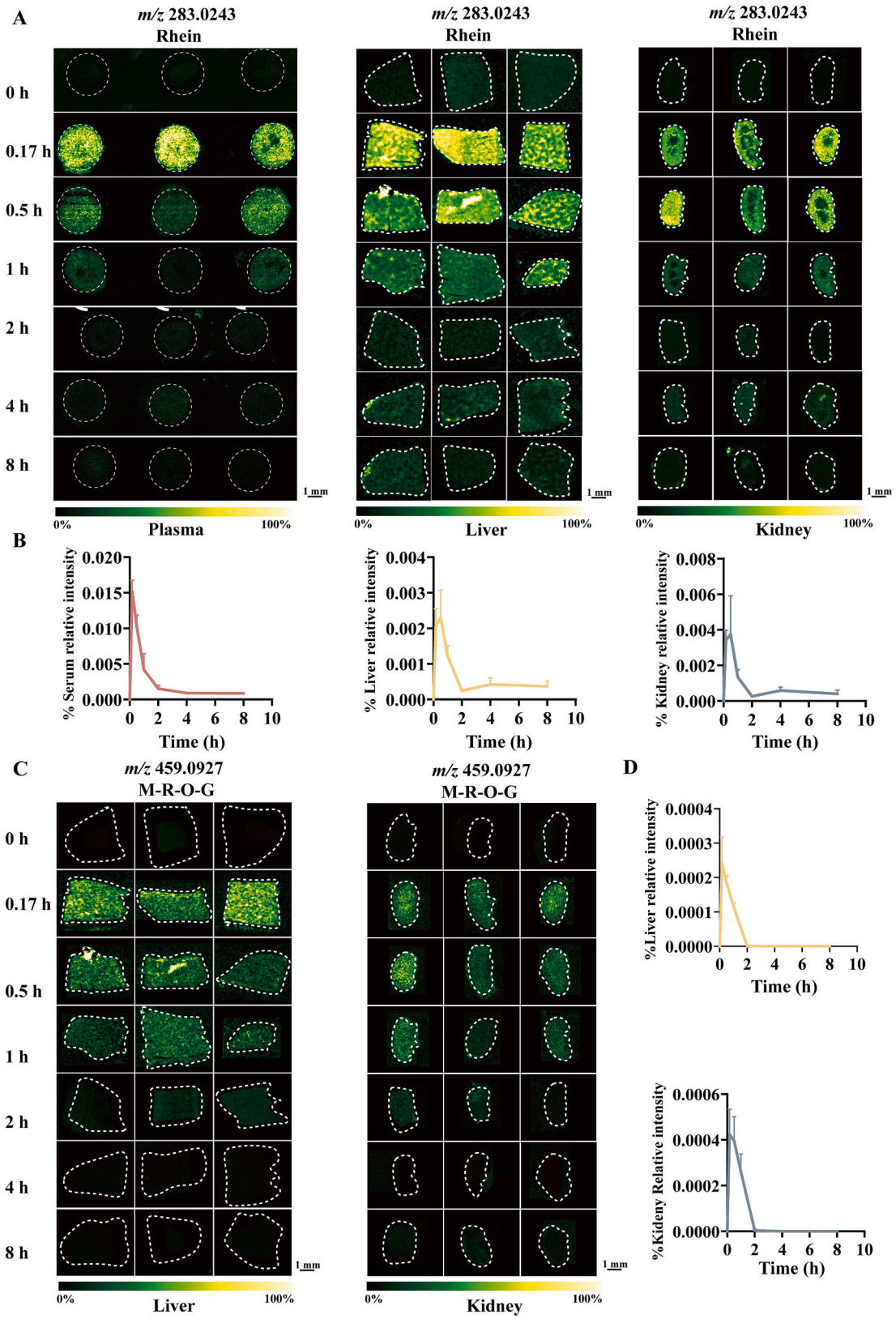

Fig. 2. Spatiotemporal alteration of rhein and its metabolite in plasma, liver and kidney ($n = 3$). (A) Representive DESI-MS images of rhein across plasma, liver and kidney sections. (B) Corresponding relative intensity of rhein in plasma, liver and kidney. (C) DESI-MS images of M-R-O-G in liver and kidney. (D) Relative intensity of M-R-O-G in liver and kidney.

3.2. Metabolic pathways of mice plasma, liver, and kidney after intervention with rhein

Metabolite profiles in plasma, liver, and kidney were analyzed at 0.17 h and 8 h post-dose in negative ion mode and compared with the blank group. PCA (Figs. S4A, S5A, and S6A) revealed favorable clustering phenomena at both time point, confirming analytical accuracy and data reliability. Given the complexity of the biological information of the metabolome, attributing it to a single factor can be challenging. Therefore, OPLS-DA was applied to further analyze the two groups of samples. Figs. S4B show good inter-group discrimination, indicating that R2 = 0.791 and Q2 = -0.628 after 0.17 h of oral administration, whereas R2 = 0.254 and Q2 = -0.695 after 8 h of oral administration. The comparison of the liver is shown in Fig. S5B, indicating that R2 = 0.933 and Q2 = -0.324 after 0.17 h of oral administration, whereas R2 = 0.912 and Q2 = -0.404 after 8 h of oral administration. The comparison of the kidney is shown in Fig. S6B, indicating that R2 = 0.392 and Q2 = -0.533 after 0.17 h of oral administration, whereas R2 = 0.889 and Q2 = -0.333 after 8 h of oral administration. The model demonstrated good grouping and predictive performance. A comprehensive analysis of metabolites in model classification (VIP > 1) highlighted distinct differences in metabolites under the negative ion mode across plasma, liver, and kidney.

Enrichment analysis was conducted on potential biomarkers to evaluate whether specific metabolic pathways, chemical classed, or biological functions were significantly enriched in the metabolite list and to infer potential biological mechanisms (Tables S9-S14). The QEA

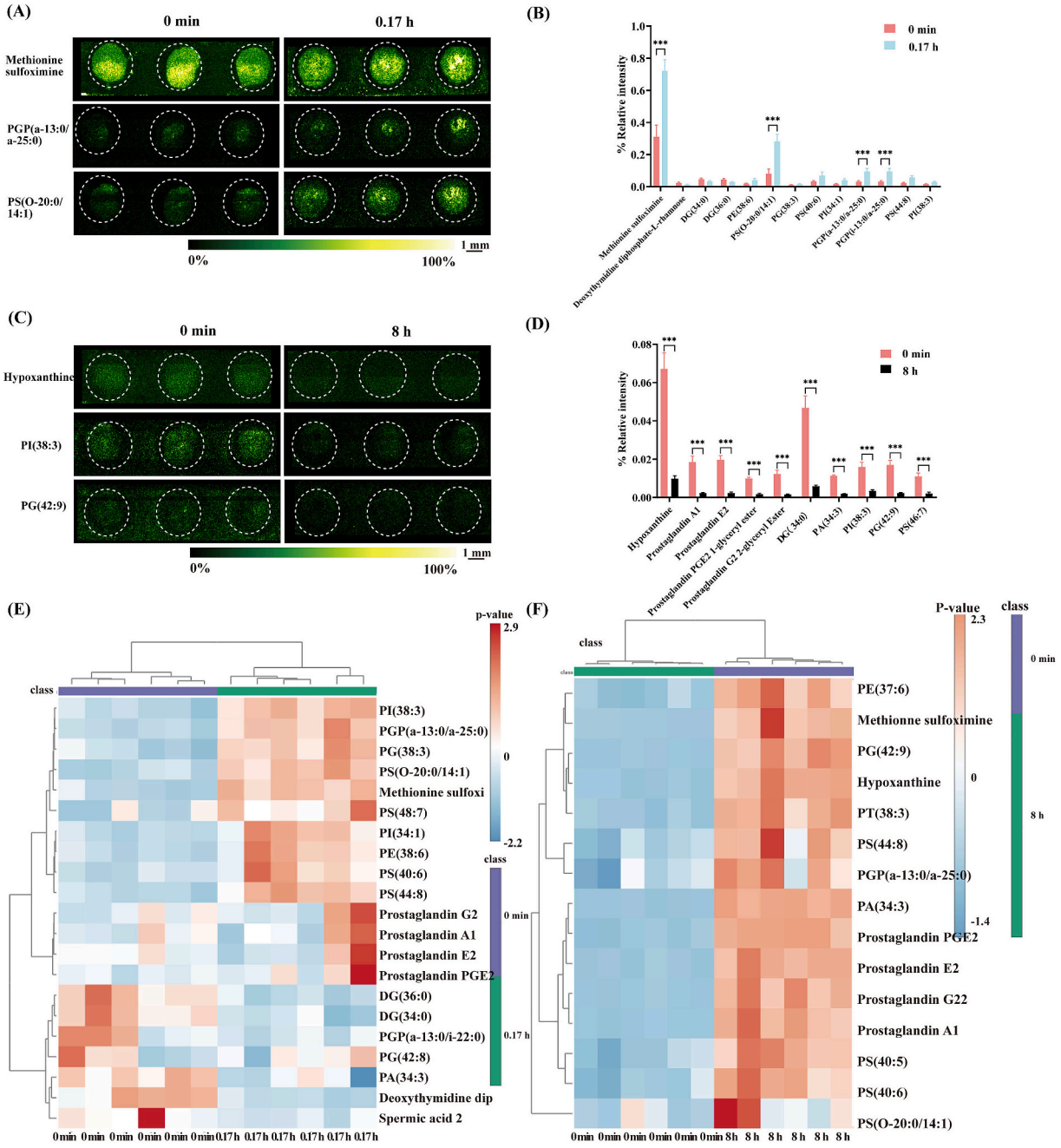

Fig. 3. Spatial metabolites analysis of rhein in plasma after oral administration. (A) Spatial distribution of different metabolites in blank and 0.17 h plasma collected 0.17 h post-dose ($n = 3$). (B) Corresponding relative intensity of the metabolites in 0.17 h *vs* blank (C) Spatial distribution of different metabolites inblank and plasma collected 8 h post-dose ($n = 3$). (D) Relative intensity of the metabolites at 8 h *vs* blank ($n = 3$). (E) Heat map of metabolite levels in blank and 0.17 h plasma ($n = 3$). (F) Heat map of metabolites in blank and 8 h liver ($n = 3$).

method was used to identify the enriched metabolic pathways with $P < 0.05$. The significance of pathways and the number of metabolites were represented by bar plots and bubble plots. After intragastric administration of rhein for 0.17 h and 8 h, the changed metabolic pathways in plasma were cysteine and methionine metabolism and cytochrome P450 metabolism pathway (Figs. S4C and S4E), the changed metabolic pathways in liver were arachidonic acid metabolism, caffeine metabolism, cysteine metabolism, amino acid metabolism, and cytochrome P450 metabolism (Figs. S5C and S5E), while the changed metabolic pathways in the kidney were tryptophan metabolism, caffeine metabolism, glycine, serine and threonine metabolism, and cytochrome P450 metabolism (Figs. S6C and S6E).

For KEGG pathway enrichment analysis of potential biomarkers, multiple significant KEGG terms were obtained by screening according to the pathway impact value from high to low with $P < 0.05$ (Tables S15-S20). After oral administration for 0.17 h and 8 h, the changed metabolic pathways in plasma were phosphatidylglycerol metabolism, linoleic acid metabolism, cytochrome P450 metabolism, and arachidonic acid metabolism (Figs. S4D and S4F), the changed metabolic pathways in liver were glycerophospholipid metabolism, taurine metabolism, α-linolenic acid metabolism, tryptophan metabolism, and arachidonic acid metabolism (Figs. S5D and S5F), and the changed metabolic pathways in kidney were tryptophan metabolism, glycerophospholipid metabolism, glycine metabolism and cytochrome P450 metabolism (Figs. S6D and S6F).

3.3. Metabolic changes in mice after oral administration of rhein

MSI technology clearly illustrate the tissue architecture and *in-situ* spatial distribution of metabolites. Fatty acids serve as both energy sources and components of membranes, and they exert bioactive effects that modulate cellular and tissue metabolism, function, and responses to hormones and other signals [23]. Rhein, a major substance regulating lipid metabolism, inhibits pancreatic lipase, reduce fat synthesis, stimulate fat breakdown, and modulate the expression of lipid-related factors, thereby promoting lipid reduction [24]. Using DESI-MSI, we compared metabolite changes in plasma, liver, and kidney of the treated group after 0.17 h and 8 h of oral administration with those of blank group. As shown in Figs. 3A-3D and Tables S21-S22, 21 and 17 spatially resolved plasma metabolites were detected at 0.17 h and 8 h, 13 metabolites were identified. After 0.17 h of oral administration, 10 metabolites were upregulated and 3 downregulated with VIP > 1 (Fig. 3B). Compared with the blank group, PS (O-20:0/14:1(9Z)), PGP (a-13:0/a-25:0), and PGP (i-13:0/a-25:0) were identified as the main upregulated spatial differential lipid metabolites, together with a significant change in methionine sulfoximine. At 8 h,10 plasma spatial metabolites were upregulated **(**VIP > 1, Fig. 3D**)**, DG (34:0), PA (34:3), PI (38:3), PG (42:9), and PS (46:7) were identified as the principal upregulated spatial differential lipid metabolites. Plasma levels of hypoxanthine, prostaglandin A1, prostaglandin E2, prostaglandin PGE2, and prostaglandin G2was significantly altered (Fig. 3C**)**. As shown in Fig. 4A, B and Tables S23-S24, DESI-MSI detected 50 and 39 spatial resolved liver metabolites at 0.17 h and 8 h, respectively. At 0.17 h, 23 liver metabolites were selected as the differential metabolites, including 13 upregulated and 10 downregulated with VIP >1 (Fig. 4E). Compared with the blank group, PG (36:2) and PI (18:0/20:3) were upregulated, whereas FAHFA (40:8), LysoPI (20:4), PE (36:3), PG (36:2), PI (18:0/20:3), PS (40:5), PE (36:2), and PI (34:0) were downregulated spatial differential lipid metabolites. N-Myristoyl serine, as a metabolite in the plasma, was significantly altered (Fig. 4C). At 8 h, 21 liver metabolites were upregulated and 4 were downregulated with VIP > 1 (Fig. 4F). N-lauroyl proline, N-lauroyl valine, cis-4-decenoyl carnitine, and succinylcholine were identified as upregulated spatial differential metabolites, while FAHFA (18:1/18:0) was downregulated (Fig. 4D). As shown in Fig. 5A, B and Tables S25, S26, 108 and 56 kidney metabolites were detected at 0.17 h and 8 h, respectively, 86 were upregulated with VIP > 1 (Fig. 5E). Compared with the blank group, tryptamin, purine, uric acid, succinylcholine, PE (38:4), PG (36:2), PS (42:6), and PC (33:1) were identified as upregulated spatial differential lipid metabolites (Fig. 5C). At 8 h,33 differential metabolites were observed: 28 were upregulated, and 5 were downregulated with VIP > 1 (Fig. 5F**)**. Urea aspartate, N-lauroyl valine, PS (36:1), PC (36:4), PS (38:3), and PS (44:8) were upregulated, whereas LysoPE (20:4), lysoPI (18:0), and TG (36:0) were downregulated (Fig. 5D).

Moreover, several lipid types significantly increased. The distribution of lipids in the plasma and liver, which are homogeneous tissues lacking distinct zones, was not evident. However, the kidney possess distinct zones, and the distribution of lipids in kidneys was notable. After 0.17 h post-dose, in PEs, upregulated PE (36:4) and PE (44:9) localized in the renal medulla. In PIs, upregulated PI (36:0) and PI (40:5) distributed in the renal medulla. PEtOH (44:9) acculated in the pelvis. At 8 h post-dose, downregulated LysoPE (20:4) and LysoPI (18:0) were found in both renal cortex and medulla. In TGs, downregulated TG (36:0) was restricted to the renal medulla. In PSs, upregulated PS (36:1), PS (38:3), and PS (44:8) distributed in both renal medulla and pelvis. In PCs, upregulated PC (36:4) distributed in the renal cortex and medulla.

Accumulating evidence indicates that lipid metabolism is a key driver of liver and kidney fibrosis progression [25,26]. In chronic fibrosis states, glucose and amino acid metabolism patterns are markedly reprogrammed [27]. PC and PE are recognized as the most prevalent phospholipids in the cell membrane. Abnormal high or low PC/PE molar ratios in cells of various tissues can influence energy metabolism [28]. PS is required for appropriate inter-dual-layer distribution of cholesterol, hepatic PS depletion causes cholesterol to accumulate in the plasma membrane [29]. Meanwhile, TG serves as the crucial role in cellular energy storage and metabolism, reduced TG intensity may indicate a reduced diminished energy demand [30]. So analysis of representative mRNA associated with the lipid metabolism were verified combined MSI data with metabolomics in the subsequent study.

3.4. The impact of oral administration of rhein on lipid metabolism

To investigate the effect of oral administration of rhein on lipid metabolism, we analyzed the mRNA expression levels of FASN, PLIN2, PPAR-α, PPAR-γ, and SCD1(Fig. S7A-S7E). During the fatty acid synthesis stage, FASN and SCD1 catalyze the synthesis of saturated fatty acids. PPAR-γ promotes adipocyte differentiation and PLIN2 stores lipids [31]. Meanwhile, after activation, PPAR-α promotes the breakdown of TG in lipid droplets. After oral administration of rhein for 0.17 hand 8 h in liver tissues, the result showed a significant up-regulation of PPAR-α (Fig. S7C). The expression of FASN showed a down-regulation after 8 h in liver tissues (Fig. S7A). Furthermore, after oral administration of rhein for 0.17 h and 8 h in kidney tissues, PPAR-γ showed a down-regulation level. The data indicated that oral administration of rhein may affect lipid metabolism.

4. Conclusion

In summary, this study successfully developed and validated an analytical methodology for rhein and its metabolites by integrating LC-MS/MS and DESI-MSI techniques. Pharmacokinetic analysis revealed that rhein undergoes rapid absorption into systemic circulation, hepatic metabolism, and subsequent renal excretion. Spatial distribution mapping demonstrated that rhein was initially localized predominantly in the renal cortex before progressively accumulating in cortical and medullary regions over time. Spatial metabolomics further indicates that the use of rhein may cause disruptions in phospholipid metabolism in liver and kidney. Meanwhiles, the spatial distribution of endogenous metabolites in the kidney is specific. Combining endogenous metabolites can explore potential mechanisms and metabolic pathways. The KEGG enrichment pathways show that the use of rhein may also have an impact on amino acid and carbohydrate metabolic pathways. Compared

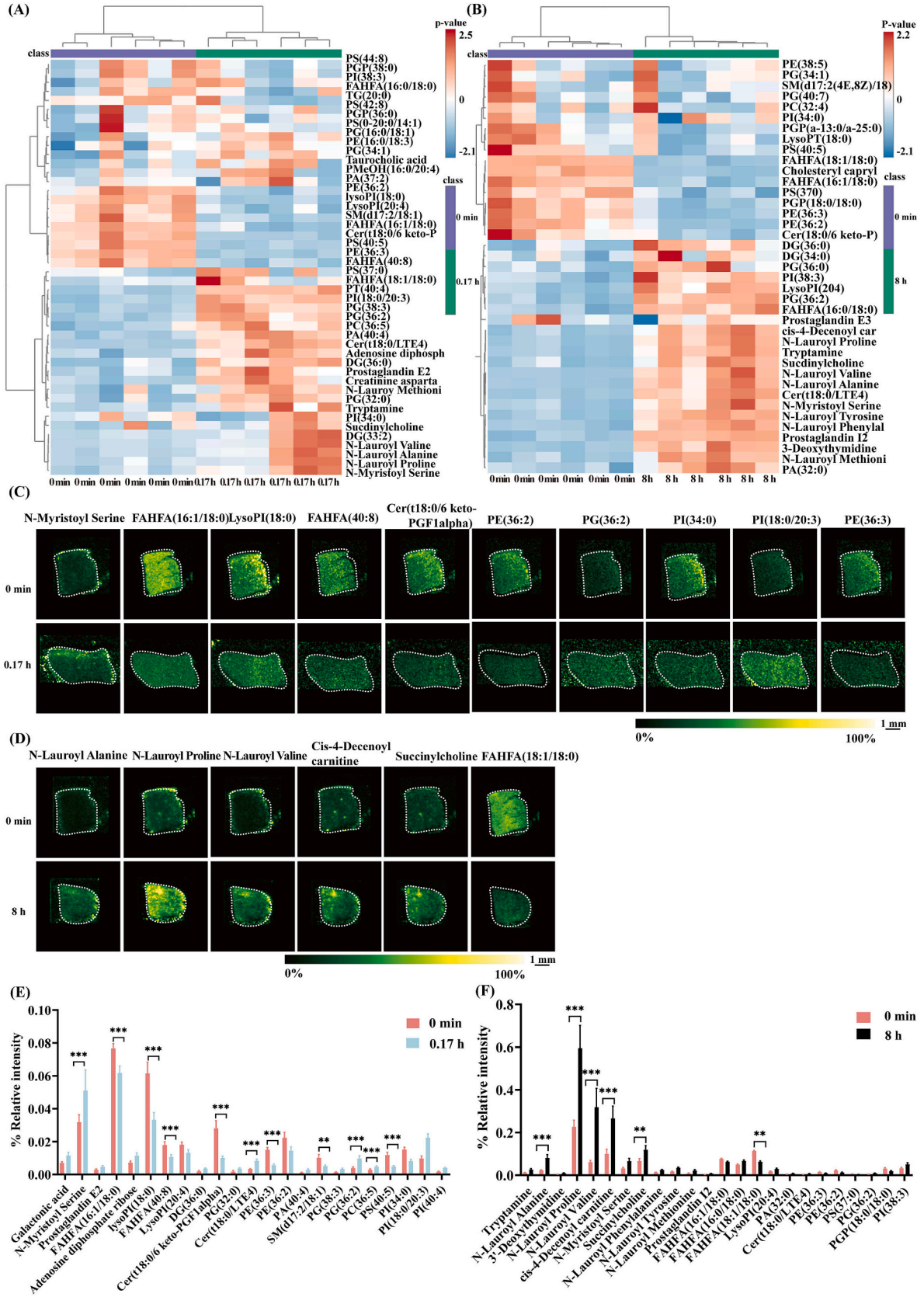

Fig. 4. Spatial metabolites analysis of rhein in the liver after oral administration. (A) Spatial distribution of different metabolites in blank and liver collected 0.17 h post-dose ($n = 3$). (B) Corresonding relative intensity of metabolites at 0.17 liver *vs* blank. (C) Spatial distribution of different metabolites in blank and liver collecte at 8 h post-dose ($n = 3$). (D) Relative intensity of metabolites at 8 h liver *vs* blank ($n = 3$). (E) Heat map of different metabolites in blank and 0.17 h liver ($n = 3$). (F) Heat map of different metabolites in blank and 8 h liver ($n = 3$).

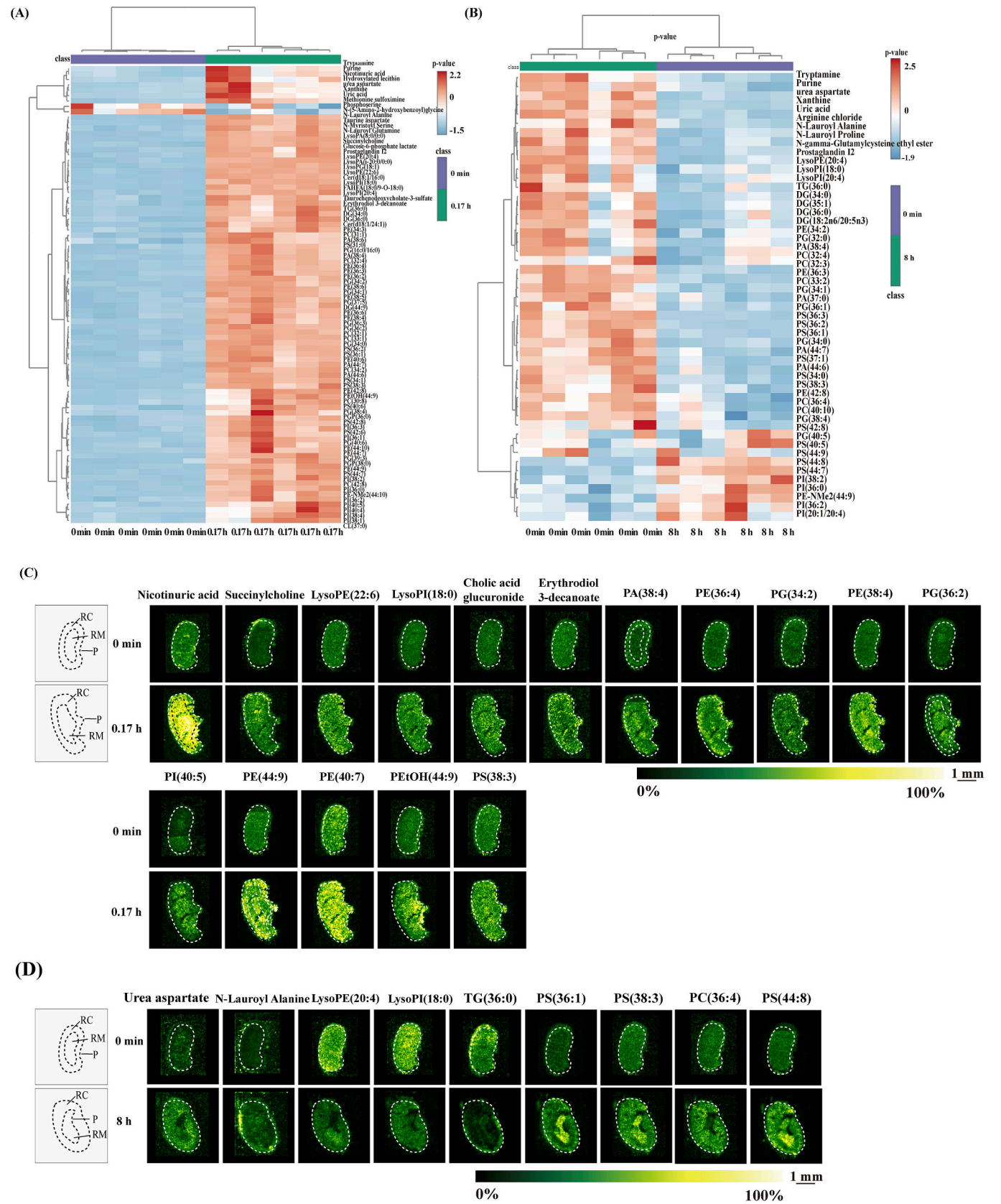

Fig. 5. Spatial metabolites analysis of rhein in the kidney after oral administration. (A) Spatial distribution of different metabolites in blank and kidney collected 0.17 h post-dose ($n = 3$). (B) Corresponding relative intensity of the metabolites at 0.17 h kidney *vs* blank ($n = 3$). (C) Spatial distribution of different metabolites in blank and kidney colledted 8 h post-dose ($n = 3$). (D) Relative intensity of the metabolites at 8 h kidney *vs* blank ($n = 3$). (E) Heat map of different metabolite levels in and 0.17 h kidney ($n = 3$). (F) Heat map of different metabolite levels in blank and 8 h kidney ($n = 3$). RC: renal cortex, RM: renal medulla, P: renal pelvis.

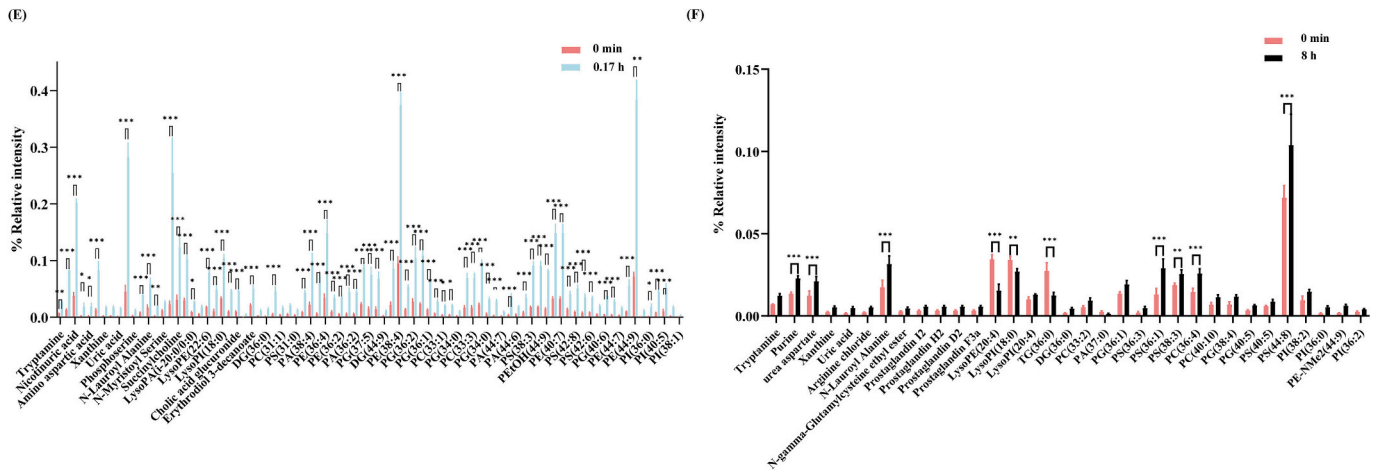

Fig. 5. (*continued*).

with traditional metabolomics, through MSI data, metabolic information can be obtained at one time. Moreover, analyzing the correlation between endogenous metabolites and the spatial distribution characteristics of rhein is a key point for the in-depth mining of future imaging data. It will provide more beneficial information on the mechanism of compounds. The representative mRNA associated with the lipid metabolism indicated that oral administration of rhein may affect lipid metabolism. LC-MS/MS can provide quantitative data on the concentrations of drugs and their metabolites, while DESI-MSI can visually display the drugs and endogenous metabolites in space. The combination of these two techniques can be used in future drug development to evaluate the spatial pharmacokinetics.

CRediT authorship contribution statement

Qin Shen: Writing – review & editing, Writing – original draft, Validation, Methodology, Investigation, Formal analysis. **Longhui Zhang:** Investigation, Formal analysis. **Chuting Xu:** Investigation, Formal analysis. **Guosheng Fu:** Investigation, Formal analysis. **Qinying Feng:** Investigation, Formal analysis. **Yongli Wang:** Formal analysis. **Chaoqun Zhao:** Formal analysis. **Wenna Ma:** Formal analysis. **Hong Xu:** Writing – review & editing, Supervision, Project administration, Formal analysis. **Wei Liu:** Writing – review & editing, Supervision, Project administration, Formal analysis. **Jing Hu:** Writing – review & editing, Supervision, Project administration, Formal analysis.

Declaration of competing interest

The authors declare that they have no known competing financial interests or personal relationships that could have appeared to influence the work reported in this paper.

Acknowledgments

We gratefully acknowledge financial support from the National Natural Science Foundation of China (No. 82474045); Shanghai Rising-Star Program supported by Shanghai Science and Technology Committee (24QA2709200), the Shanghai Natural Science Foundation (24ZR1467100); the Three-year Action Plan for Shanghai TCM Inheritance, Innovation and Development Program (ZY (2025-2027)-3-1-1), Shanghai Oriental Talents-Technology Platform Program (QNWS2024054); Science Research Project of Hebei Education Department (QN2025437); the Open Fund of Hebei Technological Innovation Center of Chiral medicine (ZXJJ20240204); Science and Technology Development Project of Shanghai University of Traditional Chinese Medicine (23KFL048); the Opening Project of Shanghai Key Laboratory of Compound Chinese Medicines (Shanghai University of Traditional Chinese Medicine) (21DZ2270500), the Health and Family Planning Research Project of Pudong New Area Health and Family Planning Commission (PW2022D-12), Pilot Project of Inheritance, Innovation and Development of Traditional Chinese Medicine in Pudong New Area (YC-2023-0602).

Appendix A. Supplementary data

Supplementary data to this article can be found online at https://doi.org/10.1016/j.microc.2026.117277.

Data availability

Data will be made available on request.

References

[1] T. Venit Shelton, Transplanted: Chinese herbal medicine in the United States, 1800-1911, Chin. Med. Cult. 6 (2023) 357–366, https://doi.org/10.1097/mc9.0000000000000 087.
[2] S.Y. Ma, J.L. Liu, W.H. Li, et al., Machine learning in TCM with natural products and molecules: current status and future perspectives, Chin. Med. 18 (2023) 43, https://doi.org/10.1186/s13020-023-00741-9.
[3] T. Zeng, J.H. Li, R.B. Wu, Natural product databases for drug discovery: features and applications, Pharm. Sci. Adv. 2 (2024), https://doi.org/10.1016/j.pscia.2024.1 00050.
[4] S.M. Khan, M. Amjad, R. Shakil, et al., Diacerein's role in alleviating inflammation and synovial effusion in knee osteoarthritis: a novel therapeutic approach, Med. Adv. 3 (2025) 54–56, https://doi.org/10.1002/med4.70004.
[5] C.S. Shen, Z.G. Zhang, T. Xie, et al., Rhein suppresses lung inflammatory injury induced by human respiratory syncytial virus through inhibiting NLRP3 inflammasome activation via NF-kappaB pathway in mice, Front. Pharmacol. 10 (2019) 1600, https://doi.org/10.3389/fphar. 2019. 01600.
[6] H.J. Wang, D.Z. Yang, L. Li, et al., Anti-inflammatory effects and mechanisms of Rhein, an anthraquinone compound, and its applications in treating arthritis: a review, Nat. Prod. Bioprospect. 10 (2020) 445–452, https://doi.org/10.1007/s13659-020-00272-y.
[7] S. Zhuang, J. Zhong, Y.F. Bian, et al., Rhein ameliorates lipopolysaccharide-induced intestinal barrier injury via modulation of Nrf2 and MAPKs, Life Sci. 216 (2019) 168–175, https://doi.org/10.1016/j.lfs.2018.11.048.
[8] L. Wang, X.X. Yu, H.J. Li, et al., Cell and rat serum, urine and tissue metabolomics analysis elucidates the key pathway changes associated with chronic nephropathy and reveals the mechanism of action of rhein, Chin. Med. 18 (2023) 158, https://doi.org/10.1186/s13020-023- 00862-1.
[9] D.Q. Zhang, L.J. Zhang, G.F. Chen, et al., Hepatoprotective effect of Xiayuxue decoction ethyl acetate fraction against carbon tetrachloride-induced liver fibrosis in mice via inducing apoptosis and suppressing activation of hepatic stellate cells, Pharm. Biol. 58 (2020) 1229–1243, https://doi.org/10.1080/13880209.2020.1855212.
[10] S.H. Liu, R.Y. Yin, Z.W. Yang, et al., The effects of rhein on D-GalN/LPS-induced acute liver injury in mice: results from gut microbiome-metabolomics and host transcriptome analysis, Front. Immunol. 13 (2022) 971409, https://doi.org/10.3389/fimmu.2022.971409.

[11] T.C. Bu, C.Y. Wang, Q. Meng, et al., Hepatoprotective effect of rhein against methotrexate-induced liver toxicity, Eur. J. Pharmacol. 834 (2018) 266–273, https://doi.org/10.1016/j.ejphar.2018.07.031.
[12] J.S. Wu, R. Shi, X. Lu, et al., Combination of active components of Xiexin decoction ameliorates renal fibrosis through the inhibition of NF-kappaB and TGF-beta1/Smad pathways in db/db diabetic mice, PLoS One 10 (2015) e0122661, https://doi.org/10.1371/journal.pone.0122 661.
[13] R.D. Beger, T.J. Flynn, Pharmacometabolomics in drug safety and drug-exposome interactions, Metabolomics 12 (2016) 123, https://doi.org/10.1007/s11306-016-1061-2.
[14] H.X. Cao, A.H. Zhang, H.M. Zhang, et al., The application of metabolomics in traditional Chinese medicine opens up a dialogue between Chinese and Western medicine, Phytother. Res. 29 (2015) 159–166, https://doi.org/10.1002/ptr.5240.
[15] P.S. Suresh, R.K. Jairam, D.V. Chandrasekhar, et al., Prediction of human pharmacokinetics of Ulixertinib, a novel ERK1/2 inhibitor from mice, rats, and dogs pharmacokinetics, Eur. J. Drug Metab. Pharmacokinet. 43 (2018) 453–460, https://doi.org/10.1007/s13318-018-0465-y.
[16] Y.Q. Fu, L. Yang, L. Liu, et al., Rhein: an updated review concerning its biological activity, pharmacokinetics, structure optimization, and future pharmaceutical applications, Pharmaceuticals 17 (2024), https://doi.org/10.3390/ph17121665.
[17] H. Zhang, K.H. Lu, M. Ebbini, et al., Mass spectrometry imaging for spatially resolved multi-omics molecular mapping, Npj Imaging 2 (2024) 20, https://doi.org/10.1038/s44303-024- 00025-3.
[18] H.Y. Jiang, Y.X. Zhang, Z.G. Liu, et al., Advanced applications of mass spectrometry imaging technology in quality control and safety assessments of traditional Chinese medicines, J. Ethnopharmacol. 284 (2022), https://doi.org/10.1016/j.jep.2021.114760.
[19] H.H. Pang, Z.P. Hu, Metabolomics in drug research and development: the recent advances in technologies and applications, Acta Pharm. Sin. B 13 (2023) 3238–3251, https://doi.org/10.1016/j.apsb.2023.05.021.
[20] P.P. Chen, Z.H. Zhu, H.Y. Geng, et al., Integrated spatial metabolomics and transcriptomics decipher the hepatoprotection mechanisms of wedelolactone and demethylwedelolactone on non-alcoholic fatty liver disease, J. Pharm. Anal. 14 (2024) 100910, https://doi.org/10.1016/j.jpha.2023.11.017.
[21] J.W. Han, P. Li, H. Sun, et al., Integrated metabolomics and mass spectrometry imaging analysis reveal the efficacy and mechanism of Huangkui capsule on type 2 diabetic nephropathy, Phytomedicine 138 (2025), https://doi.org/10.1016/j.phymed.2025.156397.
[22] Y. Zhang, H.L. Ma, X. Mai, et al., Comparative pharmacokinetics and metabolic profile of Rhein following oral administration of Niuhuang Shang Qing Tablets, rhubarb and Rhein in rats, Int. J. Pharmacol. 15 (2018) 19–30, https://doi.org/10.3923/ijp.2019. 19.30.
[23] P.C. Calder, Functional roles of fatty acids and their effects on human health, JPEN J. Parenter. Enteral Nutr. 39 (2015), https://doi.org/10.1177/0148607115595980.
[24] L.J. Wu, X.J. Wang, J.H. Jiang, et al., Mechanism of rhubarb in the treatment of hyperlipidemia: a recent review, Open Med. 18 (2023), https://doi.org/10.1515/med-2023-0812.
[25] Z.M. Tian, M.Y. Liang, Renal metabolism and hypertension, Nat. Commun. 12 (2021), https://doi.org/10.1038/s41467-021-21301-5.
[26] J. Lee, J.-S. Park, Y.S. Roh, Molecular insights into the role of mitochondria in non-alcoholic fatty liver disease, Arch. Pharm. Res. 42 (2019) 935–946, https://doi.org/10.1007/s12272-019-01178-1.
[27] C.Y. Ung, A. Onoufriadis, M. Parsons, et al., Metabolic perturbations in fibrosis disease, Int. J. Biochem. Cell Biol. 139 (2021), https://doi.org/10.1016/j.biocel.2021.106073.
[28] J.N. van der Veen, J.P. Kennelly, S. Wan, et al., The critical role of phosphatidylcholine and phosphatidylethanolamine metabolism in health and disease, Biochim. Biophys. Acta Biomembr. 1859 (2017) 1558–1572, https://doi.org/10.1016/j.bbamem.2017.04.006.
[29] M. Maekawa, G.D. Fairn, Complementary probes reveal that phosphatidylserine is required for the proper transbilayer distribution of cholesterol, J. Cell Sci. 128 (2015) 1422–1433, https://doi.org/10.1242/jcs.164715.
[30] P.S. Xie, J. Chen, Y.J. Xia, et al., Spatial metabolomics reveal metabolic alternations in the injured mice kidneys induced by triclocarban treatment, J. Pharm. Anal. 14 (2024), https://doi.org/10.1016/j.jpha.2024.101024.
[31] V. Dubois, J. Eeckhoute, P. Lefebvre, et al., Distinct but complementary contributions of PPAR isotypes to energy homeostasis, J. Clin. Invest. 127 (2017) 1202–1214, https://doi.org/10.1172/JCI88894.